

## FAST observations of ion solitary waves

J. P. McFadden,<sup>1</sup> C. W. Carlson,<sup>1</sup> R. E. Ergun,<sup>2</sup> F. S. Mozer,<sup>1</sup> L. Muschietti,<sup>1</sup> I. Roth,<sup>1</sup> and E. Moebius<sup>3</sup>

Received 13 May 2002; revised 20 February 2003; accepted 4 March 2003; published 30 April 2003.

[1] Measurements from the FAST spacecraft are used to show that ion solitary waves observed at the lower edge of the acceleration region travel at velocities faster than the associated auroral proton beams. The parallel phase velocity is consistent with the acoustic speed in the reference frame of the proton beam, strongly suggesting these waves are an ion acoustic mode. Their high phase velocity places them outside the ion beam population and rules out the ion two-stream instability as their source. These low-altitude structures may arise out of turbulence generated at the lower edge of the acceleration region. Their preferential observation at FAST altitudes may result from their high velocity combined with weak Landau damping that is restricted to the tenuous hot plasma sheet ions near the loss cone. Three different methods for estimating the velocity of these structures are examined. For the FAST antennae configuration it is found that signal delays between Langmuir probes operated in either current mode or voltage mode cannot provide valid estimates of the velocities. Instead, velocities are estimated by measuring the energy shift in the electron distribution within the negative potential well of the solitary wave. Using the measured wave potential and electric field, the scale size and velocity of the structures are calculated. Asymmetric solitary waves, sometime described as weak double layers, are also examined and shown to have no significant net potential. These new velocity estimates contrast sharply with reports based upon Viking observations and differ by about a factor of 2 from recent estimates deduced from Polar observations. These results are discussed in the context of previous estimates along with possible sources of error. *INDEX TERMS:* 2483 Ionosphere: Wave/particle interactions; 2772 Magnetospheric Physics: Plasma waves and instabilities; 2704 Magnetospheric Physics: Auroral phenomena (2407); 2736 Magnetospheric Physics: Magnetosphere/ionosphere interactions; *KEYWORDS:* solitary wave, ion hole, weak double layer, density cavity, acoustic mode, ion beam

**Citation:** McFadden, J. P., C. W. Carlson, R. E. Ergun, F. S. Mozer, L. Muschietti, I. Roth, and E. Moebius, FAST observations of ion solitary waves, *J. Geophys. Res.*, 108(A4), 8018, doi:10.1029/2002JA009485, 2003.

### 1. Introduction

[2] Ion solitary waves and weak double-layer like structures were first observed by the S3-3 satellite in association with upgoing ion beams and accelerated electrons [Temerin *et al.*, 1982]. Ion solitary waves are symmetric bipolar parallel electric field structures with typical amplitudes of  $\sim 10$  mV/m and characteristic periods of 3–10 ms. The term “weak double layer” refers to a similar electric field structure with an asymmetric bipolar signature indicating a possible net potential drop across the structure. These structures are also referred to as “ion holes” since they represent a localized ion density depletion in the plasma.

They should not be confused with “electron solitary waves” [Ergun *et al.*, 1998a], sometimes called “fast solitary waves” or “electron holes,” which are associated with electron beams. In this paper we will not distinguish between the symmetric and asymmetric bipolar signatures and will refer to these structures collectively as ion solitary waves.

[3] The importance of ion solitary waves to energy transport and energy exchange between particles, or as a support mechanism for anomalous resistivity and parallel electric fields, has been a topic of much speculation. The initial S3-3 measurements were unable to determine the velocity of the structures (they were estimated to be traveling  $>50$  km/s [Temerin *et al.*, 1982]), and thereby determine properties of the wave mode. Subsequent observations by the Viking satellite led to reports of solitary wave velocities that were much smaller ( $\sim 10$  km/s) than the associated ion beam velocities ( $\sim 100$ – $400$  km/s) [Bostrom *et al.*, 1988, 1989]. This posed a theoretical problem since the long timescale mode should be an ion mode, yet the waves traveled much slower than the measured ion beams. The problem seemed to be solved

<sup>1</sup>Space Sciences Laboratory, University of California, Berkeley, California, USA.

<sup>2</sup>Laboratory for Atmospheric and Space Physics, University of Colorado, Boulder, Colorado, USA.

<sup>3</sup>Department of Physics, University of New Hampshire, Durham, New Hampshire, USA.

when a separate population of cold, slowly moving ions was reported within the acceleration region [Koskinen *et al.*, 1990]. These ions were reported to have  $\sim 10$  times the density of the energetic ion beams and to be drifting up the field line. In addition, Langmuir probe current measurements suggested that a cold ( $\sim 10$  eV) electron population was also present with about the same density as the reported cold ion component [Koskinen *et al.*, 1990]. The combined measurements seemed to provide a self-consistent picture of these structures. The relatively small amplitude of the calculated wave potentials made it unlikely that these structures played any significant role in the auroral acceleration.

[4] Recent observations by the FAST satellite have called into question the cold plasma measurements by Viking. Both direct measurements of the plasma density [McFadden *et al.*, 1999a] and inferred limits to the cold electron density based upon wave dispersion [Strangeway *et al.*, 1998; Ergun *et al.*, 1998b] show that any cold population is less than 20% of the ion beams' density, with measurements consistent with no cold components. In addition, Cattell *et al.* [1998], Bounds *et al.* [1999], and Dombeck *et al.* [2001] have reported much higher velocities ( $>100$  km/s) for solitary wave structures using delay times between voltage measuring Langmuir probes on the Polar satellite. Dombeck *et al.* [2001] report that the ion solitary waves propagate at velocities comparable to the proton beam. The Polar technique differs from that used on Viking, where, in the latter case, delays in signals from current measuring Langmuir probes were used.

[5] In order to resolve this problem, detailed measurements of ion solitary waves were examined using both current probe and voltage probe measurements on the FAST satellite. As shown below, these techniques give conflicting values for solitary wave velocities. The problem is resolved by detailed measurements of the electron distribution function. These observations show measurable shifts in the electron spectra within the solitary wave structures that are only consistent with structures propagating faster than the proton beam. The high velocity of these structures also has implications on their generation and rules out the ion two-stream instability [Bergmann and Lotko, 1986] as the source of these low-altitude waves. The paper concludes with a discussion of asymmetric solitary waves and a possible generation mechanism for these structures. If the reader wishes to avoid a discussion of technical problems associated with Langmuir probes, we suggest skipping to section 5.

## 2. Instrumentation

[6] The electric field experiment on the FAST satellite consists of four radial antennae wires, each containing two spherical sensors, and two axial stacer antennas [Ergun *et al.*, 2001]. A deployment failure in one of the radial antennae produced a geometry depicted in Figure 1. The remaining sensors still provide a 3-axis electric field measurement, although with reduced sensitivity in one axis of the spin plane. The asymmetry of the deployment prevented us from using the Polar technique [Dombeck *et al.*, 2001] for measuring solitary wave velocities. Electric field observations are derived from voltage differences between antennae

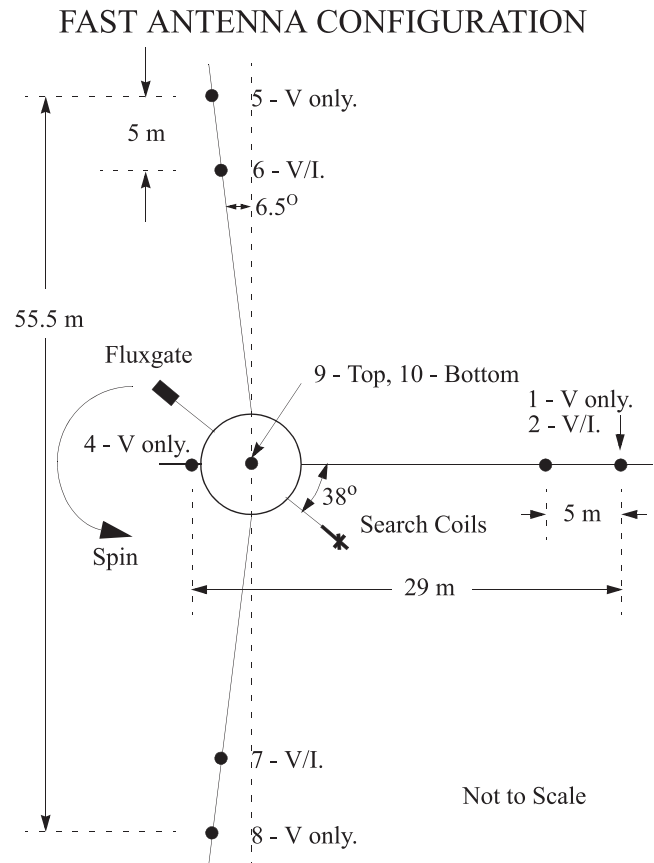


**Figure 1.** A three-dimensional view of the electric and magnetic field sensors on the FAST satellite. The electric field instrument has eight spherical sensors that are on four spin plane wire booms (two each) and two that are on rigid axial booms. The wire boom carrying sensors 3 and 4 did not fully deploy. All of the spherical sensors can operate in “Voltage Mode,” marked with “V,” in which they measure the local plasma potential with respect to the payload. Six of the ten sensors, marked with “I,” can operate in current mode where the electron current is measured for deriving plasma density. The spin plane electric field signals can be measured by various pairs of sensors which form dipole antennae varying from 5 to 56 m.

sensors, with a large number of different antennae combinations simultaneously available at sample rates up to 32 kHz. The radial antennae contain two sensors located 23 m and 28 m from the spacecraft spin axis. Both sensors can be operated in voltage mode with selectable bias currents; however, the inner sensors can also be operated in current mode with a fixed bias voltage. The different antenna combinations allow for high sensitivity measurements by the long baseline antenna, or short antennae measurements that can be used to estimate wavelengths or propagation velocities.

[7] The plasma experiment on FAST consists of 16 electrostatic analyzers organized into 8 pairs covering all pitch angles [Carlson *et al.*, 2001]. Two of the pairs provide complete electron (EESA) and ion (IESA) pitch angle distributions from 4 eV to 30 keV (25 keV for ions) with

78 ms resolution. The remaining 6 pairs (SESA) measure electron pitch angle distributions at 6 selectable energies every 1.6 ms. Selection of the energy levels can be fixed, or onboard algorithms can be used to select an energy range based upon characteristics of the most recent measured distribution. These high-time resolution measurements are used to observe changes in the electron distribution on timescales of the solitary wave structures. Mass composition is provided by a time-of-flight mass spectrometer [Klumpar *et al.*, 2001].

### 3. Problems With Velocity Estimates Using Langmuir Probes in Voltage Mode

[8] The conflicting results between the Viking [Koskinen *et al.*, 1990] and Polar [Cattell *et al.*, 1998; Bounds *et al.*, 1999] estimates of ion solitary wave velocities motivated an examination of the solitary wave velocities measured by FAST. An initial attempt was made to resolve the ion solitary wave velocity from signal delays between voltage-mode operated dipole antennae separated along the magnetic field, as was performed on Polar data. The antennae configuration suitable for this study is shown in Figure 1, and requires the 5, 6, 7, and 8 probes to be aligned along the magnetic field. Measured time delays between the V5-V6 and V7-V8 signals can be combined with the 50 m antennae separation to determine parallel phase velocity. As shown below, this method does not provide a satisfactory estimate of ion solitary wave velocities due to a distortion of the electric field signal.

[9] Figure 2 shows an example of ion solitary waves using voltage-mode and several combinations of antenna probes to resolve the waveforms. The long baseline antennae that are symmetric about the spacecraft (V5-V8, V6-V7) measure a relatively symmetric solitary wave signal, while the short antennae (V5-V6, V7-V8) record a distorted waveform. The distorted waveforms prevent accurate cross correlation analysis to determine the phase velocity of the waves. However, a crude estimate of the delay can be obtained from the difference in the zero crossing times in the center of the waveforms. These delays are much less than the characteristic period of the wave indicating a phase velocity that is consistent with Polar observations and much faster than was estimated for Viking observations. In Figure 2, the zero crossings in the center of the largest waveform are all within a few tenths of a millisecond, indicating a phase velocity  $>150$  km/s. We also point out that the signal delays are less than one tenth the characteristic period of the wave ( $\sim 5-6$  ms). This is important for comparison with phase velocity estimates using signal delays between probes operated in current mode, as was applied to the Viking data. We note that the Polar satellite has a different antennae geometry that does not experience these large signal distortions when calculating voltage signal delays.

[10] The short antenna distortion is not understood but is likely caused by a wave-induced change in the photoelectron current to the spherical probes, which effectively acts as a change in the sphere bias current. Other possible sources of the distortion, such as radial spacecraft fields or fields from the antennae wires, are too small to produce the observed distortion. The sphere bias currents on FAST

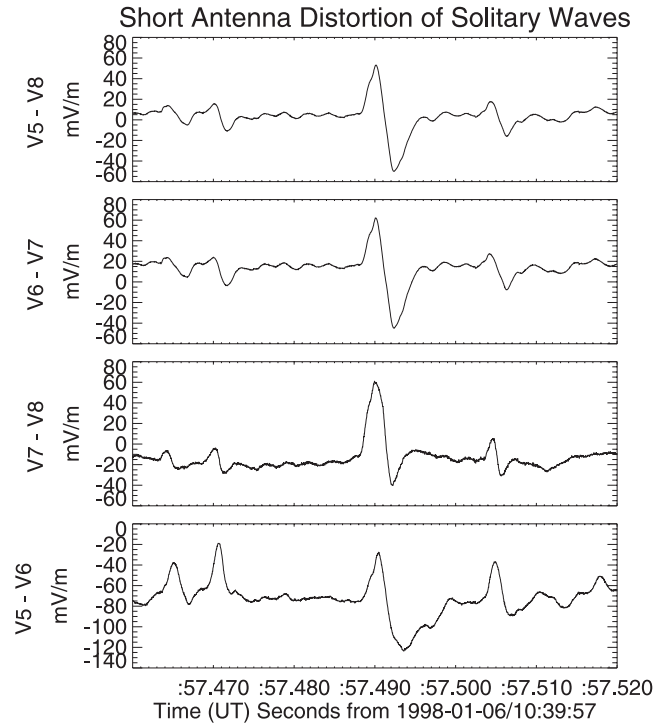


**Figure 2.** The upper two panels show that the long antennae measure relatively symmetric solitary wave structures. The bottom two panels show that the short antennae signals are distorted by a poorer signal-to-noise ratio which prevents accurate interferometry. The signal distortions are believed to be caused by changes in the photoelectron currents to the antennae sensors induced by the waves. Orbit 5441.

were set relatively low when compared to other missions (Polar, Cluster) in order to prevent spacecraft charging. For low bias currents, proper operation requires that other time-varying antennae currents be negligible or cancel due to symmetric antennae pairings. It appears that for the short antennae sphere-stub-guard geometry on FAST, the changes in photoelectron current induced by the solitary waves creates changes in the sphere to plasma potential that are comparable to the small wave potential differences for closely separated spheres. The long antennae measurements have a factor of  $\sim 10$  larger wave potential difference between spheres, so the time-varying photoelectron currents produce a minimal distortion of the wave.

[11] In support of the photoelectron interpretation of the distortion, we point out that even the long antenna signals show low-frequency (multiples of spin period) distortion as the antennae rotate through the magnetic field. These distortions are caused by a cloud of spacecraft photoelectrons confined to motion along the magnetic field. The level of distortion depends upon the plasma conditions and antenna orientation. From measurement of the Langmuir probe current, the photoelectron fluxes are slightly reduced when the spacecraft is within the low-density cavities associated ion solitary waves, as compared to outside the cavities. This is because the spacecraft must attract back more of its photoelectrons for current balance. However, as shown below, the photoelectron fluxes remain the dominant

current to the probes when the probes are field aligned. When the probes are operated in voltage mode, the photoelectron currents will be less than those measured in current mode, but still represent a significant current of low-energy electrons to the probe. This strongly suggests that the waveform distortion is due to wave-induced changes in these photoelectron currents, which act as a bias current change that affects the probe to plasma potential.

#### 4. Problems With Velocity Estimates Using Langmuir Probes in Current Mode

[12] An alternate method used to estimate solitary wave velocities is performed by measuring the delay between current spikes to Langmuir probes that are aligned along the magnetic field [Bostrom *et al.*, 1988]. The FAST electric field experiment (Figure 1) can be operated with probes 6 and 7 biased at a positive voltage while the current to the probes are measured [Ergun *et al.*, 2001]. This has an advantage over the Viking geometry in that it affords a simultaneous measurement of the electric field signal by the outer probes (V5-V8). Figure 3 shows an example of ion solitary waves measured using the combined voltage and current mode techniques. The top panel resolves the parallel component of the electric field waveform with the long antenna (V5-V8), whereas panels 2 and 3 show changes in current collected by probes 6 and 7. These current spikes are similar to those observed by Viking, showing a large  $\sim 50\%$  reduction in current and a time delay equal to half the characteristic period of the solitary wave. These large current spikes are not directly due to changes in ambient plasma density, but are due to changes in photoelectron

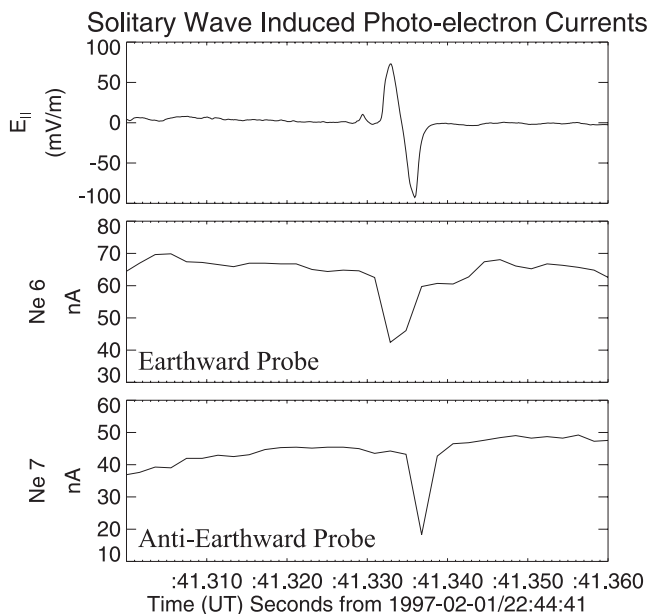


**Figure 3.** Changes in the current to Langmuir probes induced by a solitary wave. The dominant current to the probes are spacecraft produced photoelectrons. The current decreases are due to changes in these photoelectron currents. The delay between current spikes is equal to half the wave period and does not represent a propagation delay. Orbit 1779.

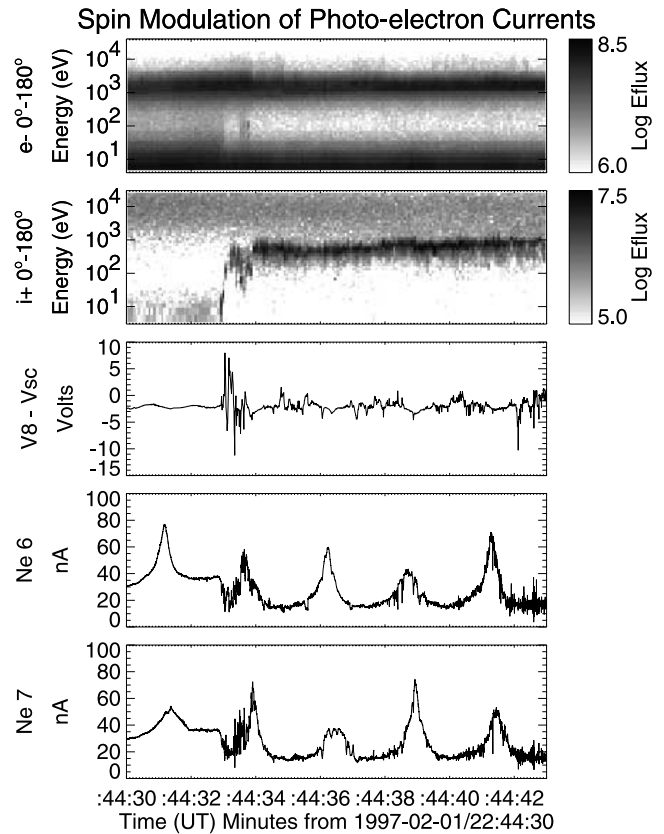


**Figure 4.** The upper panels are spectrograms of the electrons and ions as the FAST satellite enters an ion beam. The center panel shows the antennae to spacecraft potential. The bottom panels show the twice per spin modulation of the current to Langmuir probes as the probes rotate through the spacecraft photoelectron cloud which is confined along the magnetic field. Orbit 1779.

collection. Below we discuss some of the various current signals to these probes, including an attempt by FAST to avoid one of these signals, and show that this method does not provide a reliable technique for evaluating plasma density variations. We do not question that these probes measure changes in current associated with the waves, but instead demonstrate that the interpretation of the measured current is difficult, making this technique unreliable for measuring propagation velocities of ion solitary waves.

[13] Figure 4 shows the twice per spin modulation of the current to the Langmuir probes, with the current increasing by a factor of 3–5 when the probes are aligned along the magnetic field. A similar current modulation was observed on Viking and was explained by enhanced photoelectron collection when the positively biased Langmuir probes were aligned along the magnetic field [Hilgers *et al.*, 1992]. The photoelectrons originate on the antenna wire and spacecraft surfaces. Since the bulk of the probe current is due to photoelectrons when the antennae are aligned along the magnetic field, the large changes in probe current must be due to changes in photoelectron collection. Thus these current spike delays represent an interaction between the solitary wave electric field and the photoelectrons traveling along the antennae wires, not the wave's density perturba-

tion. Therefore these current spikes cannot be directly used to estimate solitary wave velocities.

[14] A detailed study of the probe's response to the solitary wave's electric field is beyond the scope of this paper; however, we note some general features of this response. The solitary wave electric field is in the correct sense to retard photoelectrons and produce the observed drop in current. During the first and second half of the wave, the spacecraft-antenna system is immersed in relatively uniform earthward and antiearthward directed electric field, respectively. The wave's electric field reduces the photoelectron current collected by the earthward probe during the first half of the wave, and reduces the current to the antiearthward probe during the second half. This produces a delay in the current spikes equal to half the wave period, as is observed in the data. A solitary wave electric field of  $\sim 60$  mV/m (Figure 3) produces a  $\sim 1.4$  V drop between the plasma near the probe and spacecraft, which could produce a significant change in spacecraft photoelectrons reaching the probe. The largest ion solitary waves have amplitudes of  $\sim 400$  mV/m, so a  $\sim 9$  V potential drop may be present between the spacecraft and probe which would dramatically affect the collection of photoelectrons.

[15] Although the photoelectron current dominates the above signals, two additional signals are present: a real current due to the change in plasma density and a capacitively coupled current due to changes in plasma to probe potential. A reduction in the probe current will be present due to the decreased electron density in the ion hole. As we will show later, the largest solitary waves have potentials the order of  $-400$  V, while the electron temperature is  $\sim 2$  keV (see orbit 1804 below). Assuming the solitary wave behaves as an acoustic mode with a density-potential relation given by the Boltzmann relation, we estimate the largest density perturbations to be  $\sim 20\%$ . A typical electron flux to the probe is  $\sim 3 \times 10^8/\text{cm}^2\text{-s}$ , producing a  $\sim 10$  nA current to the 8 cm diameter probe. Thus the largest amplitude waves only make  $\sim 2$  nA current changes. For the smaller amplitude wave of Figure 3, the current signal due to the density perturbation is  $< 1$  nA. Thus currents due to density perturbations are insignificant compared to the measured current signals. However, the solitary wave density perturbation does reduce the electron flux to the spacecraft, which will cause the spacecraft to become more positive relative to the plasma in order to attract back its photoelectrons. This will reduce the flux of escaping photoelectrons along the magnetic field and will cause a unipolar reduction in the photoelectron flux captured by the probes. The magnitude of this reduction would depend upon details of the photoelectron spectrum but might be expected to be the order of the electron density perturbation, which is generally much less than the measured current perturbations.

[16] Capacitive signals arise from voltage changes between the probe and local plasma associated with the wave. These changes depend upon details of voltage bias applied to the current probe. Typically a current probe is voltage biased relative to the spacecraft, so a bipolar voltage signal is observed between the plasma and the probe as a solitary wave passes. For a moderate signal as in Figure 3, a simple calculation ( $I = i\omega VC$ ) results in an expected bipolar current signal with amplitude of  $\sim 7$  nA. In an attempt to minimize these capacitive signals on FAST, the voltage bias

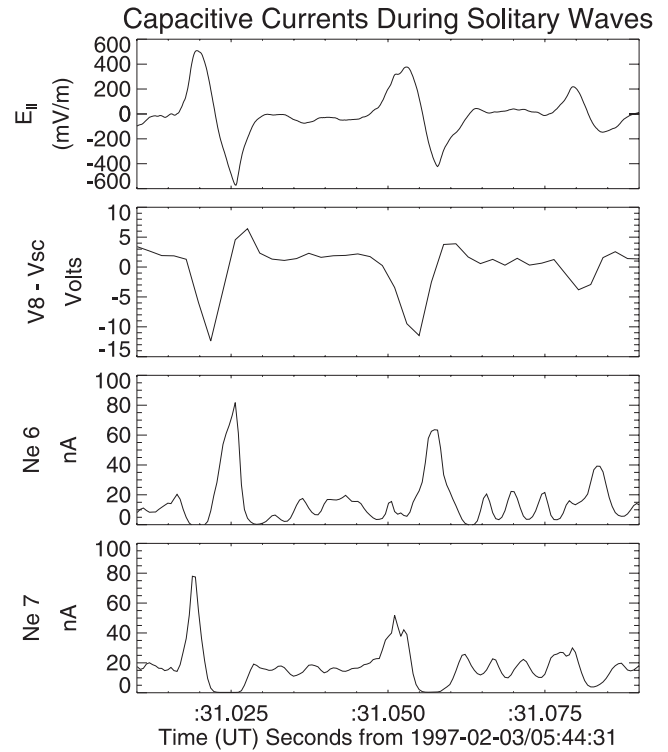


**Figure 5.** The upper panel shows some of the most intense ion solitary waves observed by FAST. The second panel shows that these intense waves produce large voltage differences between the sensors and the spacecraft. These voltage differences produce capacitively coupled currents in the Langmuir probes as shown in the bottom panels. The log amplifier in the sensor prevents measurement of a negative current from the sensor. At this time the sensors are outside the spacecraft photoelectron cloud so the dominant current perturbations are due to capacitive coupling. Orbit 1793.

was selected to be a positive offset voltage ( $V_{\text{offset}} \sim 7.5$  V) referenced to the plasma potential at the probe [Ergun *et al.*, 2001]. The plasma potential at the probe was estimated from the spacecraft potential,  $V_{\text{sc}}$ , and outer probe potential,  $V_{\text{outer}}$ , to be  $0.2V_{\text{sc}} + 0.8V_{\text{outer}}$ . The voltage tracking was designed to operate below 300 Hz, which is just above the typical effective frequency of FAST ion solitary waves. This attempt to minimize capacitive signals on the FAST current probes was not successful. Below we show that the capacitive signals are still quite large, and can dominate the measurement when the probes are outside the spacecraft photoelectron cloud.

[17] Figure 5 shows some of the largest ( $\sim 400$  mV/m) ion solitary waves observed by FAST. During these waves, probes 5, 6, 7, and 8 were aligned within  $\sim 30$  degrees of the magnetic field and outside the spacecraft photoelectron cloud so that these currents are minimal. This wave produces a  $\sim 10$  V difference between the outer probes and the spacecraft as can be seen in 5b. The signal V8 is slightly delayed due to filtering and is asymmetric indicating the spacecraft potential does not follow the local plasma potential. The baseline currents of  $\sim 20$  nA to probes 6 and 7 in Figures 5c and 5d are consistent with the energetic electron

flux. For a  $\sim 100$  Hz characteristic frequency and 4 pF probe capacitance, we would expect the solitary wave to generate a bipolar signal of amplitude  $\sim 25$  nA, assuming the probe is voltage biased relative to the spacecraft. The actual bipolar current signals are closer to 60 nA, much larger than expected even without the voltage tracking. (Note that the current probe uses a log amplifier that does not measure negative currents from the probe.) Similar signals are observed on the current probes in the presence of large amplitude EIC waves within the auroral density cavity when the probes are perpendicular to the magnetic field and have minimal photoelectron contamination. It is clear that the voltage tracking has not eliminated capacitively coupled signals. The nature of these signals is still not understood and may require a detailed analysis of the entire electronics-antennae-photoelectron-plasma interaction.

[18] We close this section by pointing out that typical current probe signals are a combination of the two dominant signals: photoelectron and capacitive signals. The relative magnitude of the two signals depends upon many parameters including details of the antennae-electronics design, the alignment of the probes along  $\mathbf{B}$ , solar illumination angle of the spacecraft, and the energetic electron flux. The phase of these signals is such that the decrease in photoelectron current collection generally corresponds to the increase in the capacitive bipolar current, so these signals tend to partially cancel. The capacitive signal is also sensitive to the shape ( $dV/dt$ ) of the solitary wave. On FAST we have observed a wide variety of current signals during solitary waves (unipolar, bipolar, and tripolar) suggesting the relative contributions of the currents are quite complicated. The nature of these signals is clearly related to the interaction of the solitary waves with the probes; however, these signals provide no information about the velocity of these structures since the current signals are not due solely to the unipolar density decrease that propagates with the ion solitary waves.

## 5. Velocity Estimates Using Changes in the Electron Distribution

[19] The high time resolution plasma measurements on FAST offer an alternate method of determining the parallel phase velocity of ion solitary structures. FAST is capable of measuring a coarse (6 energy  $\times$  16 pitch angle) electron distribution function, “f,” with 1.6 ms time resolution, adequate to resolve changes in the electrons on the 5–10 ms timescale of the solitary waves. By measuring the energy shift,  $\Delta E$ , of the electrons within the solitary wave, one can determine the depth of solitary wave potential well,  $\Phi_{\min} = \Delta E/e$ . The wave potential at the spacecraft can also be found by integrating the electric field  $\Phi(t) = V_{\parallel 0} \int_0^t E_{\parallel} dt'$ , where  $V_{\parallel}$  is the parallel velocity of the solitary wave and assumed constant during the integration. The integration is actually a sum of the measured electric fields at 32 kHz (or 8 kHz) sampling. The potential minimum is given by  $\Phi_{\min} = \Phi(t_{\min})$ , where  $(d\Phi(t)/dt)|_{t_{\min}} = 0$ . So the parallel velocity can be determined by solving:  $V_{\parallel} = (\Delta E/e)[\int_0^t E_{\parallel} dt']^{-1}$ .

[20] To resolve the wave potential, the energy shift must be large enough to produce a measurable change in the electron count rate, which in turn depends upon the slope of the electron distribution function. For keV electron energies, the solitary wave potentials must be several hundred volts in

order to resolve the parallel velocity. Although a large volume of data was gathered by FAST since its launch, the number of events suitable for velocity estimates is rather small for a variety of reasons (most data was collected outside the ion beam regions, solitary wave amplitudes were normally small ( $< 100$  mV/m), intense EIC waves were often present, suitable electric field measurements were unavailable, particle data collection were at the wrong energies, high rate particle spectra were not always gathered during events). For the discussion below, we focus on two orbits (1804, 11666) that contained some of the largest amplitude solitary waves observed. We note that most of the ion beams that were examined (several hundred) contained some solitary waves, that solitary waves with amplitudes  $> 50$  mV/m were not uncommon, and that several tens of orbits were identified that contained solitary waves with large enough amplitudes (typically  $> 50$  mV/m) to cause statistically significant count rate shifts in the electrons. However, most of these events did not have large enough wave amplitudes to provide accurate velocity estimates, so we were forced to consider case studies of the largest events.

[21] Figure 6 shows an electron distribution function from the EESA sensor averaged over  $0^\circ$ – $68^\circ$  pitch angle (top), the corresponding differential energy flux spectra (middle), and a contour plot of the differential energy flux (bottom), during an ion beam event that contained large amplitude solitary waves. The dashed lines in the upper plots are the one count level. The electron spectral peak at  $\sim 3$ – $4$  keV is slightly broadened by averaging over time ( $\sim 0.32$  s, 4 energy sweeps) and over angle. During this period a set of six electron sensors (SESA) were operated in a fixed energy mode that measured electrons at energies including 2.4 and 4.8 keV. The negative potential well of an ion hole will shift the electron distribution function to lower energy producing an increase in the 2.4 keV count rate and a decrease in the 4.8 keV counts.

[22] Figure 7 shows observations of large amplitude solitary waves measured during the averaged distribution in Figure 6. The top two panels show the parallel and perpendicular electric field, with the parallel fields dominated by the bipolar solitary waves and the perpendicular fields showing both EIC waves and unipolar signals due to the solitary waves. Panels 3 and 4 show changes in the count rate of the 2.4 and 4.8 keV electron channels, averaged over  $0^\circ$ – $68^\circ$  pitch angle. Each solitary wave has an associated increase in the 2.4 keV electron count rate, and decrease in the 4.8 keV rate as expected for a negative potential well. The bottom three panels show the characteristic energy,  $E_{ce}$  (energy flux/number flux), of the electron distribution estimated from the counts in the 2.4 and 4.8 keV channels. The solitary waves produce a 300–700 eV shift in the electron distribution function.

[23] To obtain the energies in Figure 7, panels 5 and 6, a three second period including these data were used to make a fit of  $E_{ce}$ , calculated from the sweeping EESA sensor, versus the counts in the fixed energy sensors.  $E_{ce}$  was defined as the ratio of energy flux to particle flux, determined from a limited angle range ( $0^\circ$ – $68^\circ$ ) and limited energy range ( $.25 * E_{\text{peak}} < \text{energy} < 4 * E_{\text{peak}}$ ) centered on the spectral peak,  $E_{\text{peak}}$ .  $E_{ce}$  varied slowly during this period reflecting a small change in the inverted-V potential drop. The corresponding fixed energy channel counts were deter-

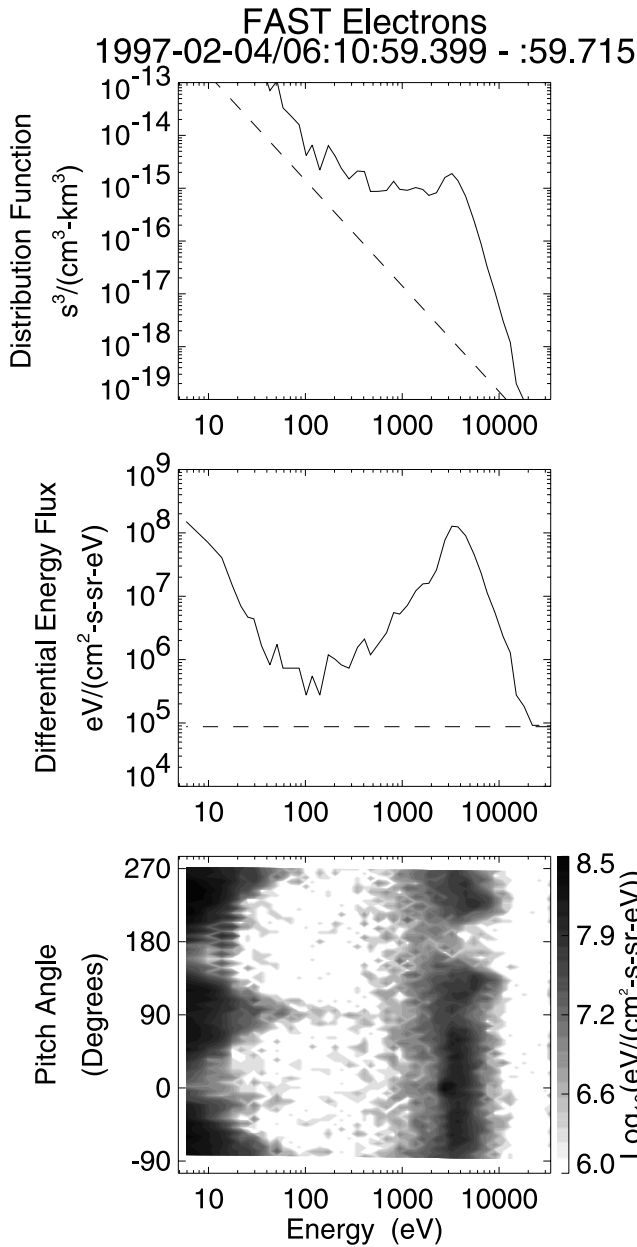


**Figure 6.** The electrons during an ion beam are plotted as distribution function, as differential energy flux, and as an angle-energy map of differential energy flux. Electrons below 100 eV are primarily spacecraft produced photoelectrons. This electron distribution corresponds to the period in Figure 7. Orbit 1804.

mined from a 5 point (8 ms) average centered on the time that the EESA spectral peak was measured (same pitch angle range). Linear fits to the scatterplot of  $E_{ce}$  versus counts were then used to determine a linear function to estimate the characteristic energy plotted in panels 5 and 6.  $E_{ce}$  was found to decrease by  $\sim 600$  eV for a factor of two decrease in 4.8 keV counts over the interval.  $E_{ce}$  was found to decrease by  $\sim 500$  eV for a factor of two increase in 2.4 keV counts over the interval. A similar result (panel 7) was arrived at by assuming the electron spectra falls logarithmically with energy above the spectral peak. The logarithmic

function was calculated from the spectra in Figure 6, where the effective temperature,  $dE/d(\ln(f)) = 933$  eV, was determined from the 4.5 keV and 5.5 keV measurement by the EESA.

[24] The general agreement between the above three methods of estimating the solitary wave potential provides some confidence that our methodology is sound. However, the linear fit below the spectral peak (panel 5) was restricted to a few events where the fixed energy channel fell at the

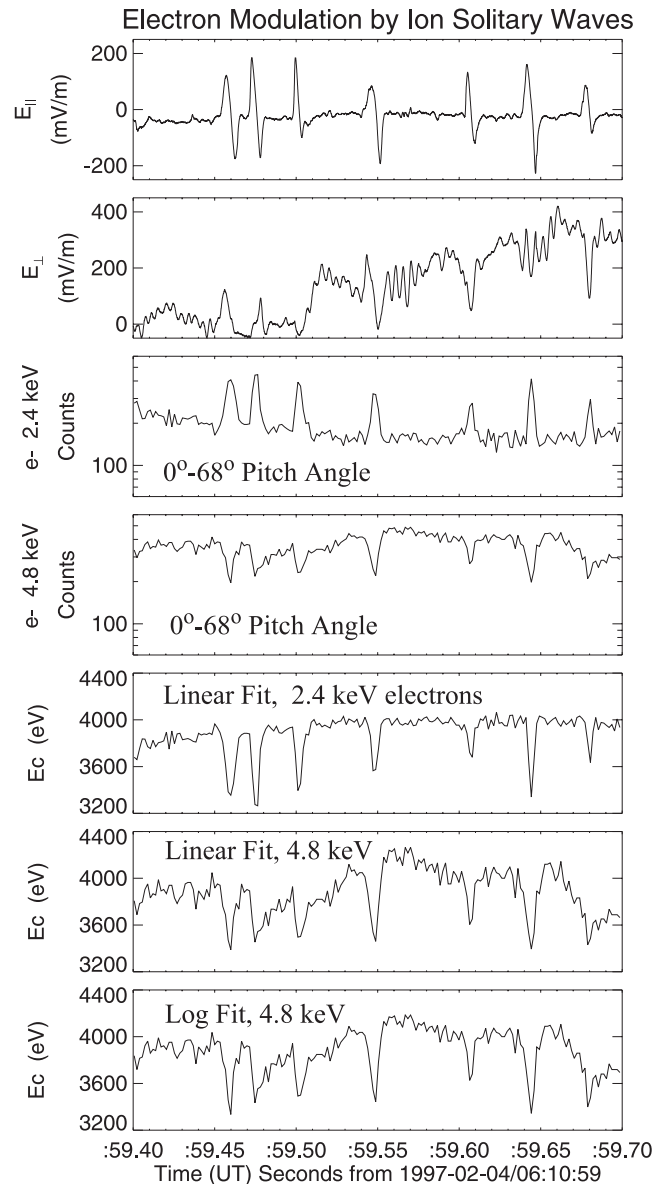


**Figure 7.** The top two panels show the parallel and perpendicular fields during a large amplitude solitary wave event. The third and fourth panels show the change in 2.4 and 4.8 keV electron counts associated with the wave. These energies correspond to the positive and negative slopes adjacent to the peak in the electron distribution function of Figure 6. The bottom three panels show the shift in the characteristic energy of the electrons estimated from the count rate shifts in the 2.4 and 4.8 keV channels. Orbit 1804.

lower-energy end of the narrow region of positive slope below the spectral peak. Therefore this method could not be used for most of the solitary waves. The agreement of log and linear fits (panels 6 and 7) partly reflects the fact that the energy shift in the distribution is a small fraction (<15%) of the measurement energy. Since the electron distribution above the spectral peak often resembles an accelerated Maxwellian, the third method was chosen for characterizing the 19 large amplitude solitary waves on FAST orbit 1804 that were found suitable for potential calculations. Several criteria were adopted in selecting the wave events. Only relatively symmetric, bipolar electric field structures whose baseline field returned to the prewave level were selected. The baseline counts in the 4.8 keV SESA sensor ( $0^\circ$ – $68^\circ$ ) had to be >170 and had to return to presolitary wave levels after the wave. In addition, the spectral peak could not be part of the energy range used for the logarithmic fit since the slope changes rapidly near the peak.

[25] Using the electron spectral shift estimate of solitary wave potential and the integrated (in time) solitary wave electric field, the parallel velocity for the 19 solitary waves were calculated. The velocities ranged from ~550–1100 km/s, with an average of 802 km/s and standard deviation of 151 km/s. Figure 8a shows a scatterplot of the wave potential versus velocity with no apparent trend. The large scatter of velocities most likely reflects several sources of error in the calculations (~10% error in  $\Phi_{\min} = \Delta E/e$  due to count rate statistics, ~10% error in  $\Phi_{\min}$  due to temporal variations in the electron spectral slope above the spectral peak, ~10% error in  $\int_0^t E_{\parallel} dt'$  due to asymmetry in the solitary waves) in addition to any real changes in velocity. Since our error estimates can account for the standard deviation in velocities, there may be no significance to this spread. Figure 8b shows a scatterplot of “potential” versus “ $\tau$ ,” the time delay between the maximum and minimum electric fields. The larger amplitude solitary waves have a larger delay time and thus a larger spatial extent. We choose to plot the time delay rather than the spatial scale size,  $V\tau$ , because the largest errors are likely in the velocity estimate; however, in Figure 8c we have included the “potential” versus “scale size” showing that larger potentials have larger scales. We caution the reader that some of the scatter in 8c may be due to errors in our determination of solitary wave velocity. Finally, since the width of the solitary waves appears to increase with amplitude, these observations suggest that these structures are not solitons [Tran, 1979], but more likely a BGK type mode as found for electron solitary waves [Muschiatti *et al.*, 1999].

[26] In an attempt to understand the range of velocities in Figure 8a, we compared velocity estimates against all measured parameters and looked for trends. There is no significant correlation of solitary wave velocity with the 0.31 second averaged ion beam characteristic energy,  $E_{ci}$ . This probably reflects the fact that  $E_{ci}$  only changes by a factor of ~2 over the events whereas rapid fluctuations in the beam on shorter timescales are present. The only correlations found were between the velocity and the effective temperature at the energy of the SESA channel, and the velocity and the count rate of the SESA measurement. These two correlations are related since the electron distribution effective temperature [ $dE/d(\ln(f))$ ] and measured count rate both decrease with energy above the spectral

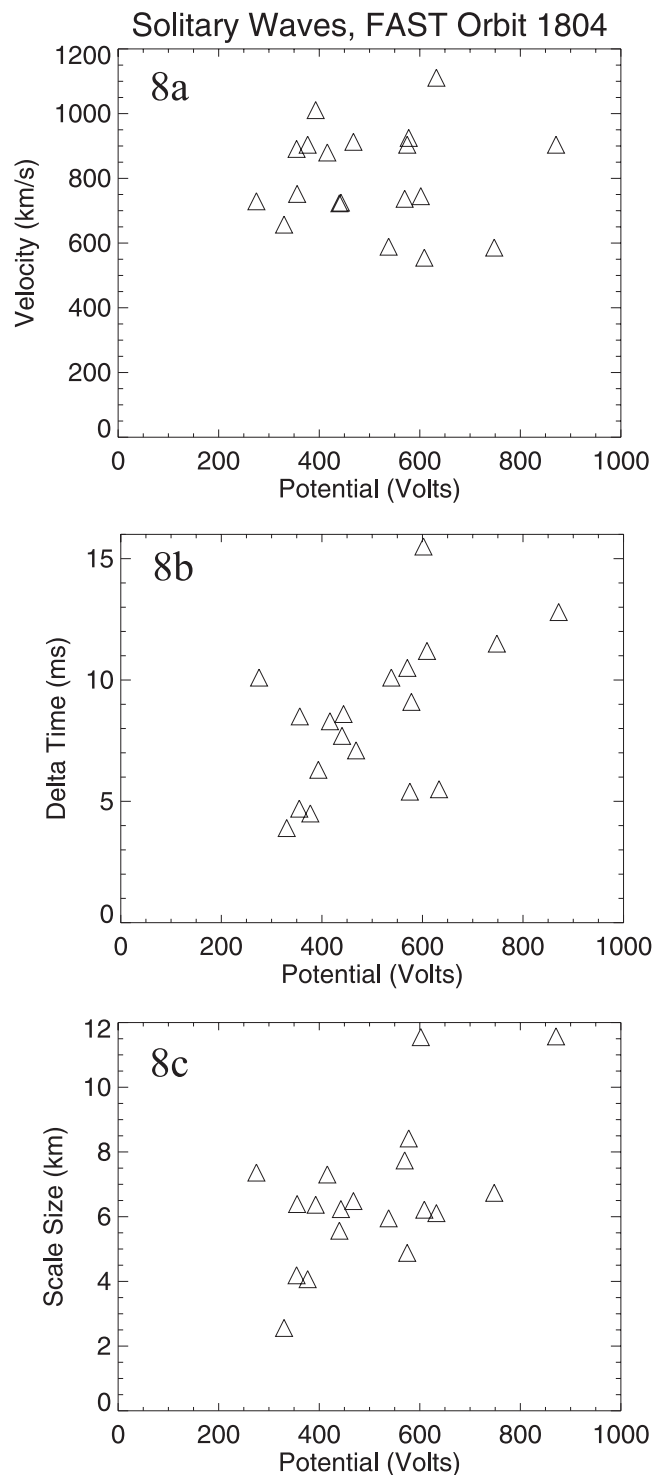


**Figure 8.** (a) Solitary wave potential versus solitary wave velocity for 19 events on FAST orbit 1804. (b) Larger amplitude events tend to have a larger duration indicating a larger spatial size. (c) Spatial size versus potential.

peak. The range of effective temperatures (662–982 eV) was not large, and some of the correlation probably reflects errors in the effective temperature measurement due to statistical fluctuations and the relatively coarse measurement of the distribution slope. We note that the three lowest

velocity measurements occurred during the 0.15 s interval with the lowest effective temperature (662 eV), and that the adjacent measured temperature averaged  $\sim 90$  eV higher.

[27] If we assume that the electron temperature above the spectral peak is constant over the interval where solitary waves are measured, and correct the velocities using an average effective temperature, we find the range of velocities decreases slightly to 594–990 km/s, with an average of 801 km/s and standard deviation of 109 km/s. Since this change is relatively small, we conclude there is no significant correlation between solitary wave velocity and any measured parameters. The spread of velocities probably reflects both statistical errors in the measurements and time variations in the plasma, in addition to the slow trends in ion energy and electron temperature during the interval. If solitary wave velocities depend upon solitary wave potential, then this dependence must be relatively weak.

[28] Using  $\tau$  time delay between the maximum and minimum electric fields, to characterize the scale size of the solitary waves (3.9 to 15.5 ms), and using the average velocity of  $\sim 800$  km/s, we estimate the half width of these structures varies between 3 km and 12 km, or  $\sim 6$ –20 debye lengths using the measured density ( $n_e \sim 0.32$  cm $^{-3}$ ) and temperature ( $T_{e\parallel} \sim 1.79$  keV) of the hot auroral electrons. Assuming a Boltzmann relation between the potential and the density perturbation, the largest density holes have a  $\sim 25\%$  drop in density. We point out that the above velocity estimate was only possible because of the large amplitude of these solitary waves. Typical solitary wave amplitudes of  $\sim 10$  mV/m would not have a significant change in the density.

[29] To compare the velocity of the solitary waves with the ion beams we need to extract the ion beam velocities from the measurements. Several measurement limitations complicate this matter. First, 2.5 second resolution measurements by the mass spectrometer are much too slow to resolve time variations in the ion beams. Instead we rely on the 78 ms resolution 2-D ion pitch angle distribution measured by the ion ESA. Figure 9 shows the ion spectra during the interval corresponding to the solitary waves in Figure 7. The protons in an auroral ion beam have a high-energy cutoff at the spectral peak and slowly decrease below, while ions measured above the peak are typically O $^+$  or He $^+$  [Moebius *et al.*, 1998]. Four sweeps were averaged to generate this relatively smooth plot. However, the characteristic energy ( $E_{ci}$ ) of the beam during these four sweeps, where  $E_{ci}$  is defined as the ratio of energy flux to particle flux, had values of approximately 2.5, 1.8, 1.9 and 2.2 keV. So the measured ion beam energy changes dramatically on 78 ms timescales. These variations are not statistical since each ion distribution had  $\sim 500$  counts, which is adequate to resolve a slowly varying beam. Instead,  $\pm 25\%$  variations in ion beam energy are observed from sweep to sweep indicating the beams are turbulent. Thus the nearest ion beam measurement to a solitary wave event is not an accurate predictor of beam properties during the event. For these reasons we decided to compare the average properties of the ion beams to the average velocity of the solitary waves.

[30] For the events in Figure 7, the average ion beam characteristic energy is  $E_{ci} \sim 2.87$  keV. A typical ion distribution during this period consists of  $\sim 0.10$  cm $^{-3}$

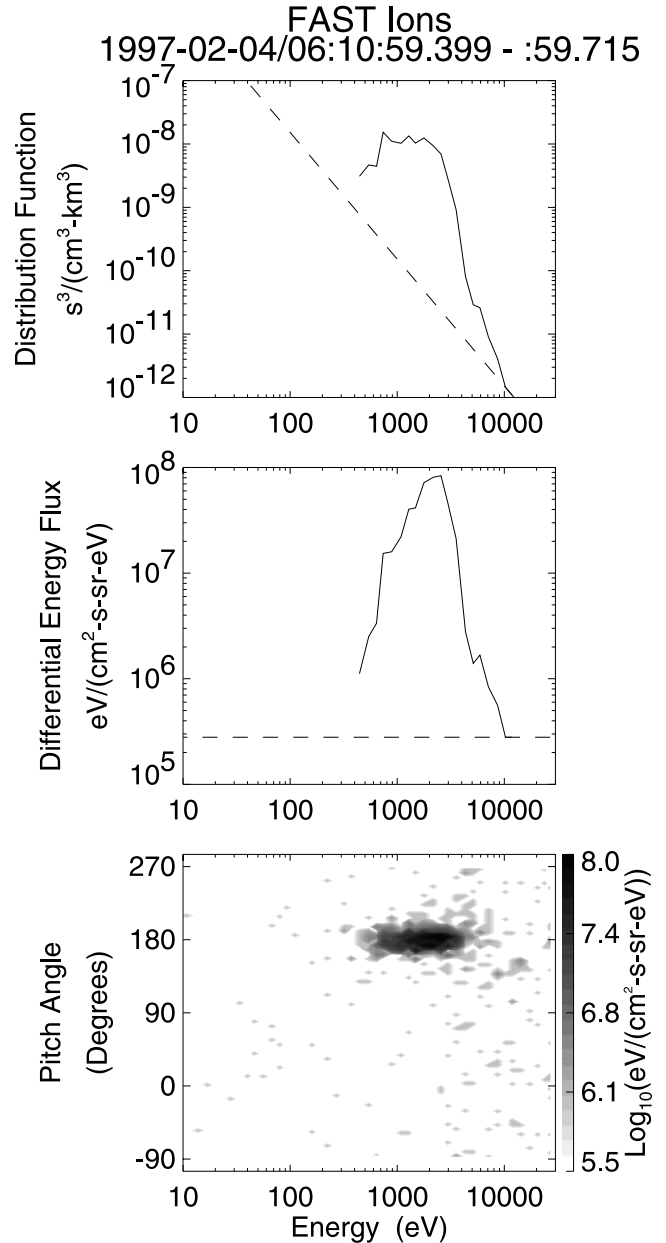


**Figure 9.** Ion beam during the solitary waves in Figure 7 are plotted as distribution function averaged over  $170^\circ$ – $190^\circ$  pitch angle and assuming only H $^+$ , as differential energy flux averaged over  $170^\circ$ – $190^\circ$  pitch angle, and as an angle-energy map of differential energy flux. Dashed lines on the upper two plots are the one count level. Orbit 1804.

plasma sheet H $^+$ , and a beam consisting primarily of H $^+$  ( $\sim 0.09$  cm $^{-3}$ ) and O $^+$  ( $\sim 0.11$  cm $^{-3}$ ), with a small amount of He $^+$  ( $\sim 0.02$  cm $^{-3}$ ). The fractional composition was determined from mass spectrometer data in an adjacent region, with absolute densities determined from the ESA. As mentioned above, the protons in an auroral ion beam have a sharp high-energy cutoff at  $\sim E_{ci}$ . Since 2.87 keV protons have a velocity of  $\sim 740$  km/s, the ion solitary waves, on average, appear to be traveling faster than the most energetic protons in the beams. The proton bulk velocity can be estimated from the moment of the ESA-

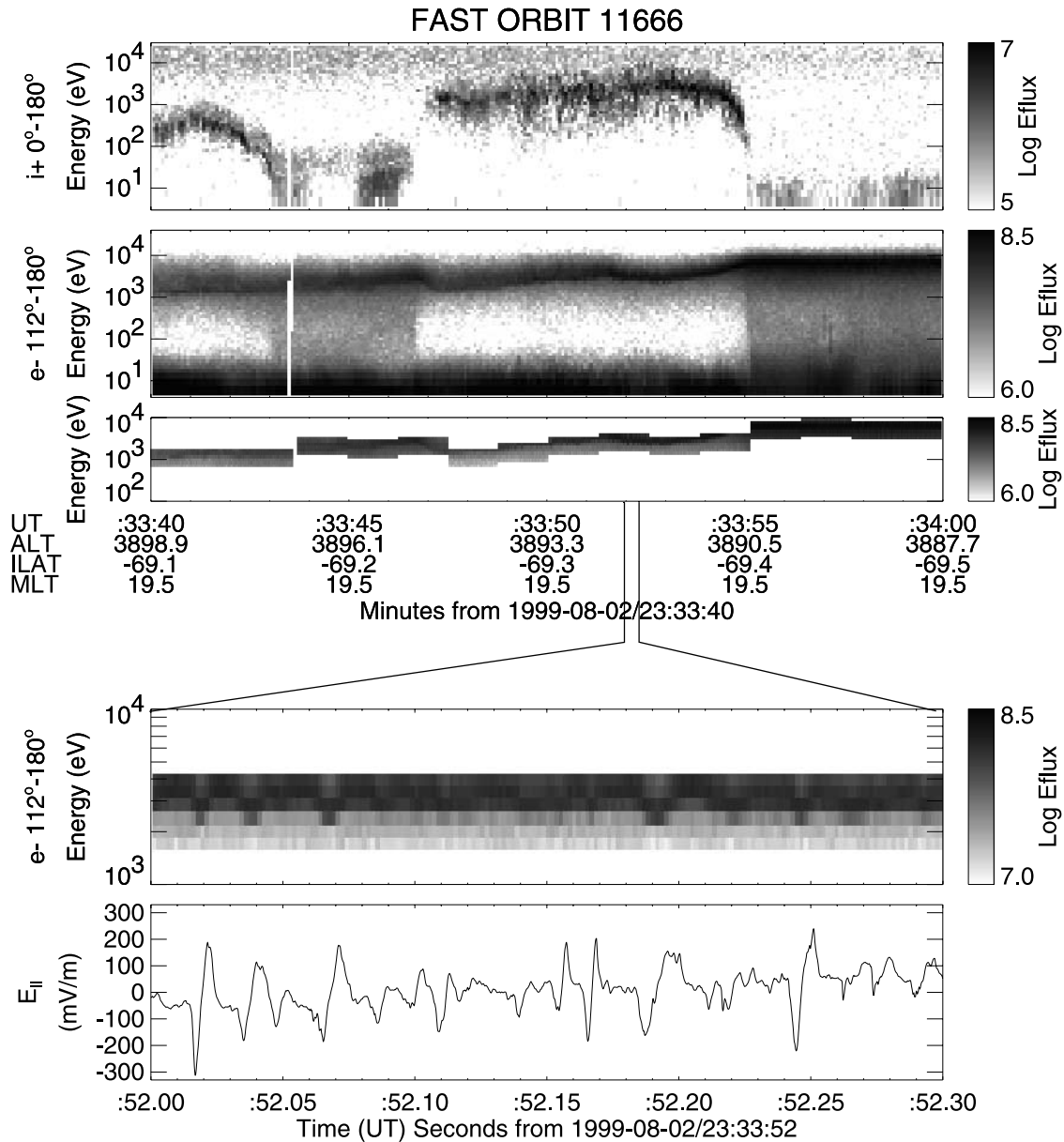


**Figure 10.** The FAST satellite passed through ion beams (panel 1) as it crossed an inverted-V electron arc (second panel). The third panel shows that the FAST SESA electron sensors were operated in a tracking mode that followed the inverted-V spectral peak. The lower panels zoom in on a stretch of data containing ion solitary waves (fifth panel). The fourth panel resolves the energy shift in the electron spectral peak associated with the solitary waves. Orbit 11666.

measured ion flux at and below the spectral peak. For this time interval, the velocity moment is typically  $\sim 0.7$  times the velocity of a proton at the characteristic energy, giving an average proton velocity moment of  $\sim 520$  km/s for the interval. Treating the proton beam as a separate cold population, its acoustic mode can be estimated to propagate at a speed of  $c_s \sim [(n_{H^+ \text{ beam}}/n_e)(T_{e||}/m_{H^+})]^{1/2} \sim 220$  km/s relative to the beam [Lotko and Kennel, 1983].

[31] This above approximation does not account properly for several features of the distribution functions (O<sup>+</sup> beam, hot plasma sheet H<sup>+</sup>, beam temperature) so we investigated numerical solutions of the dispersion relation using the WHAMP code [Roennmark, 1983] to produce a more accurate estimate of the acoustic speed. We found that most

of these features (O<sup>+</sup> beam, plasma sheet H<sup>+</sup>) were unimportant and that WHAMP reproduced the above acoustic speed as long as we assumed a cold H<sup>+</sup> beam. The FAST observations cannot resolve the proton beam temperature due to time variations, but can be used to estimate an upper limit of  $\sim 135$  eV for this event. For a H<sup>+</sup> beam temperature of  $\sim 135$  eV, we found a significant increase in the acoustic speed ( $\sim 320$  km/s), but also strong damping ( $\gamma/\omega \sim 0.15$ ). However, the protons are not Maxwellian and have a sharp cutoff at high energy. We then modeled the proton beam as 3 Maxwellians with temperatures of 50 eV, but with relative drifts of 111 km/s. This gives an effective temperature of 136 eV, but with a more box-car shape for the distribution. This produced a similar but higher  $\sim 350$  km/s acoustic

speed, but with much lower damping ( $\gamma/\omega \sim 0.03$ ). It appears that the ion beam pressure has a strong influence on the acoustic speed, and that the sharp high-energy cutoff of proton beam reduces any damping by the warm beam. Thus upgoing acoustic waves are expected to be observed at phase velocities between  $\sim(520 + 220)$  km/s and  $\sim(520 + 350)$  km/s in the spacecraft frame, depending upon the beam temperature. Therefore the ion solitary waves travel at about the correct velocity ( $801 \pm 109$  km/s) to be an acoustic mode of the proton beam. This large phase velocity assures that the waves are not damped by the beam ions but only by the more tenuous mirroring plasma sheet protons.

[32] The above events were somewhat unusual in that not only were the solitary waves large, but the electron spectral peak fell intermediate between two of the fixed SESA energy channels allowing serendipitous observations of the change in counts in two SESA channels. For most large amplitude events, statistically significant count rate shifts in the fixed energy detectors were only observed in the channel closest the spectral peak. In order to better resolve energy shifts in the distribution function peak, the FAST SESA sensor was operated for several months in a mode where the 6 sensors tracked the spectral peak in the electron distribution function. The SESA sensors remain at six closely spaced fixed energies for  $\sim 1$  s, then adjust their energy range based upon the spectral peak determined by the EESA sensor. Unfortunately only one orbit had the combination of high rate burst data, intense solitary waves, and an electron spectral peak the order of a few keV. Figure 10 shows an example of the energy tracking during this orbit, with the top two panels showing complete spectra of the electrons and ions measured by the EESA and IESA in an inverted-V arc, and the third panel showing the SESA tracking the inverted-V spectral peak. The lower two panels zoom in on a section of the data that contains ion solitary waves. Count rate shifts can be seen in up to four electron energy channels when the large amplitude solitary structures are present.

[33] Figure 11 shows a set of electron spectra ( $112^\circ - 180^\circ$  pitch angle, downgoing in southern hemisphere) measured during the passage of an ion solitary wave. The electron spectral peak shifts from  $\sim 3.2$  keV outside the structure to  $\sim 2.5$  keV inside the solitary wave. During a two second interval that included several solitary waves in Figure 10, five relatively symmetric solitary wave events, that met the criteria used in the previous analysis, were analyzed and found to have potentials (431, 540, 553, 713, and 476 volts) and velocities (868, 812, 699, 777, 647 km/s) consistent with the earlier measurements, with an average velocity of  $\sim 760$  km/s. In addition another 9 solitary wave structures, whose asymmetric shape or close proximity to other waves made them less ideal, were fit and found to have an average velocity of  $\sim 830$  km/s with standard deviation of  $\sim 260$  km/s. For the measured electron parameters ( $T_{e||} \sim 1.9$  keV,  $n_e \sim 0.4$  cm $^{-3}$ ), the time between the electric field minimum and maximum (4.7, 5.2, 6.0, 10.8, and 6.7 ms), and the average velocity ( $\sim 760$  km/s) we find the solitary waves have a scale sizes of 7–16 debye lengths, similar to the previous measurements.

[34] During these solitary wave events, the ion beam characteristic energy was  $\sim 2.6$  keV so the proton beam should have a sharp cutoff at  $\sim 700$  km/s. Thus the ion

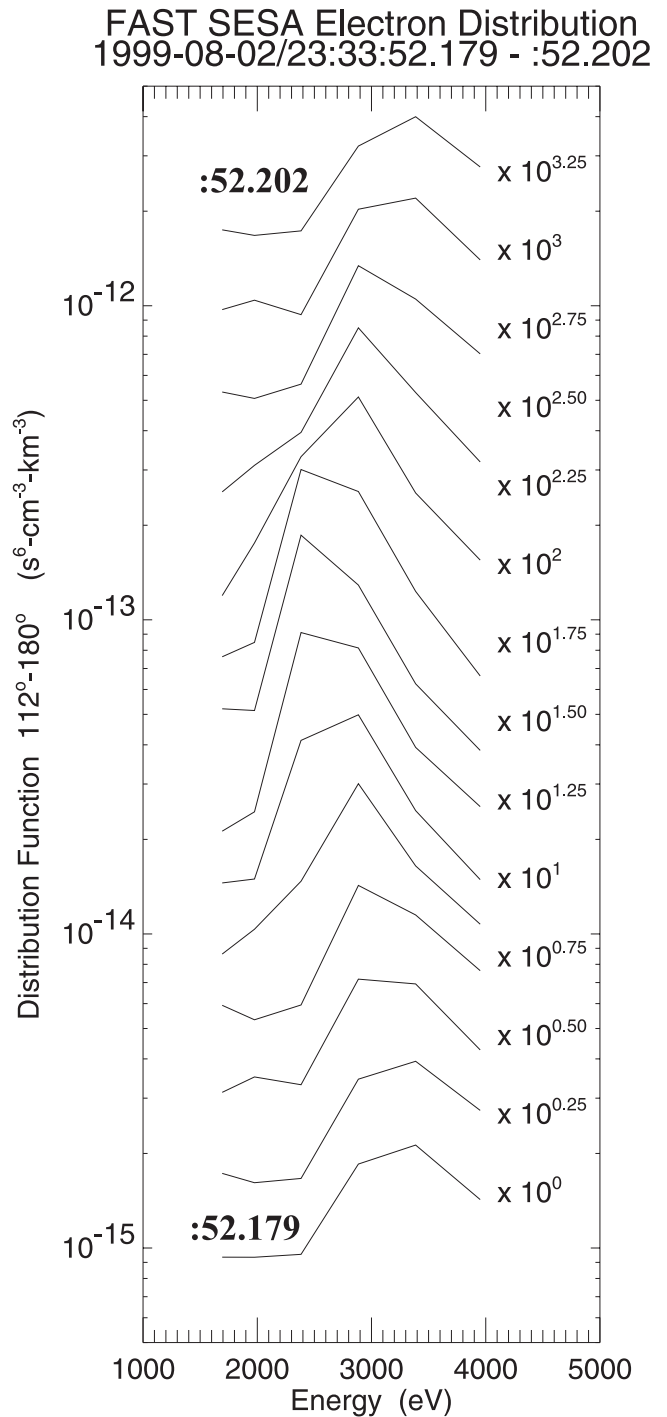


**Figure 11.** A series of electron distribution functions separated by 1.6 ms during the passage of a large amplitude solitary wave. The spectral peak is shifted down by  $\sim 700$  eV. Orbit 11666.

solitary waves are found to travel faster than the proton beam as in the previous case. To compare the wave speed with the ion acoustic speed, the beam composition and proton bulk velocity must be known. The proton bulk velocity is estimated to be  $\sim 430$  km/s from calculating the moment of the beam distribution at and below the characteristic energy where the beam is primarily H $^+$ . (If

all the upgoing ions are assumed to be  $H^+$ , the velocity moment is 500 km/s, nearly the same.) Degradation of the sensitivity of the TEAMS mass spectrometer over the first 2 years of operation progressed to a point where direct determination of the composition was not possible for field aligned beams. (The portion of the mass spectrometer's microchannel plate that observes field aligned ions suffered a substantial drop in gain, because it also encountered intense RAM  $O^+$  at low altitudes.) Instead we estimate the relative contribution of  $O^+$  from the relative fractions of the ion flux above and below the spectral peak. This method was tested by comparison with mass spectrometer data early in the mission and found to have good agreement as long as the beam energy remained constant. To provide adequate statistics, a nearby averaged distribution (23:34:05.33–:07.87) was used where the characteristic ion energy was constant. Ions at and below the spectral peak were assumed  $H^+$  and those above the spectral peak were assumed  $O^+$ . The combined densities of the  $H^+$  beam ( $0.074 \text{ cm}^{-3}$ ),  $O^+$  beam ( $0.147 \text{ cm}^{-3}$ ) and plasma sheet  $H^+$  ( $0.088 \text{ cm}^{-3}$ ) agree reasonably well with the hot electron density ( $0.339 \text{ cm}^{-3}$ ) and support our estimate that  $\sim 2/3$  of the beam density was  $O^+$ . The lower limit to the acoustic speed during the solitary waves in Figure 10 is estimated to be  $\sim 210 \text{ km/s}$  ( $T_{e\parallel} \sim 1.9 \text{ keV}$ ,  $n_e \sim 0.4 \text{ cm}^{-3}$ , beam  $H^+ \sim 0.1 \text{ cm}^{-3}$ , beam  $O^+ \sim 0.2 \text{ cm}^{-3}$ , PS  $H^+ \sim 0.1 \text{ cm}^{-3}$ ) for a cold proton beam. However, for a warm proton beam ( $\sim 150 \text{ eV}$ ), we expect an acoustic speed similar to the previous case ( $\sim 350 \text{ km/s}$ ). Therefore the expected velocity of antiearthward propagating acoustic waves in the spacecraft frame should be between  $\sim 640 \text{ km/s}$  and  $\sim 780 \text{ km/s}$ , which is consistent with estimates of the observed solitary waves and suggests they are an acoustic mode.

## 6. Asymmetric and Stretched Solitary Waves

[35] The asymmetry of the electric field signatures of solitary wave structures has been proposed as a means of producing field aligned potential drops [Temerin *et al.*, 1982; Hudson *et al.*, 1983]. Alternatively, this asymmetry could be due to evolution of the solitary waves during their transit past the antennae, due to oblique propagation of 3-D structures, or due to a real asymmetry but without a net potential drop. This latter case just requires a nonsymmetric charge distribution along the field. In addition, as discussed in sections 4 and 5, small changes in the photoelectron currents to the antennae can distort the waveforms making electric field asymmetries alone suspect in determining any implications of an asymmetry. The presence of high time resolution electron measurements on FAST allows a test for net potential drops associated with solitary waves by examining the electron flux before and after the passage of the wave.

[36] The top panel of Figure 12 shows an example of two relatively symmetric solitary waves followed by an asymmetric wave, with a fourth structure ( $\sim 06:10:58.42 \text{ UT}$ ) whose identification is less clear. Perpendicular fields of similar magnitude are observed with all the structures (second panel) indicating the 3-D nature of these waves. The lower panels show the counts in the 2.4 and 4.8 keV electron channels that straddle the energy flux peak. The counts in the symmetric solitary waves return to about the

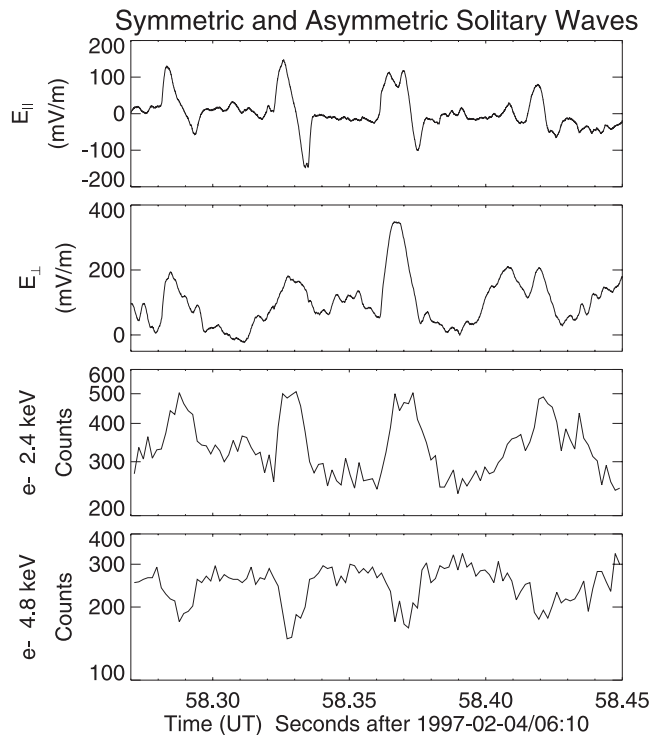


**Figure 12.** The top two panels show the parallel and perpendicular signals during several solitary wave structures. The bottom panels show the shift in electron counts associated with the waves. Both the symmetric and asymmetric structures appear to have little or no net potential since the electron counts return to prewave levels. Orbit 1804.

prewave level after each wave indicating little ( $<10\%$ ) or no net potential.

[37] The third waveform in Figure 12 is highly asymmetric indicating a possible net field aligned potential. If we assume the wave is restricted to the main oscillation between 6:10:58.360 and 6:10:58.378 UT, a net potential equal to  $\sim 80\%$  of the potential minimum (approximately  $-400$  to  $-500 \text{ V}$ ) should be observed. However, by 6:10:58.382 UT, the 2.4 keV electrons are back to prewave levels, within statistical variations. This suggests that an asymmetric charge distribution is present, and that the potential is spread out on the trailing edge. The 4.8 keV electron counts are back to prewave levels even earlier (6:10:58.378 UT) and increase to even higher levels by 6:10:58.382 UT. This is not consistent with a simple energy shift of the electron distribution due to a change in the local potential by the solitary wave, but instead indicates that the source population also has time variations. Finally, we note that the asymmetry of this solitary wave is in the wrong sense for it to carry a portion of the auroral potential drop. In active regions that contain many solitary waves, the asymmetric waveforms are about as common as the symmetric bipolar waves. In addition, there does not appear to be any preference for the polarity of the asymmetries further indicating that asymmetric solitary waves do not contribute to net potential drops.

[38] The fourth structure in Figure 12 does not have a characteristic bipolar parallel electric field signature and the electron energy shift appears to be much more spread out. In fact, the initial changes in electron counts at 6:10:58.400 appear to be associated with  $E_{\perp}$  and not  $E_{\parallel}$ . This suggests that obliquely propagating structures are also present that have associated potentials that can decelerate the electrons. The electrons appear to recover to prewave count rate levels after the turbulent fields indicating little or no net potential associated with these structures. In summary, the time variations in the electron counts appear to be primarily due to local structures propagating both parallel and oblique to the magnetic field, with some slower variations due to changes in the more distant source population.

[39] In addition to the asymmetric waveforms, some of the solitary structures appear to have a stretched shape with a wider region of plateaued potential inside. The top panel of Figure 13 shows several examples of these stretched structures. The key feature is that the parallel electric field goes through an inflection in the middle of the structure rather than showing a rapid change from positive to negative polarity as seen in the previous solitary waves. Similar stretched structures have also been observed for electron solitary waves [Muschiatti *et al.*, 2002]. The lower panels show that the electron flux again returns to the prewave level after the stretched solitary waves pass indicating no significant net potential drop.

[40] From the second panel in Figure 13, we observe that these stretched structures may or may not have significant perpendicular electric fields associated with them. Note that the large perpendicular fields in the last two structures are not centered on the electron flux changes, whereas the parallel field structure is centered. This again indicates there may be oblique propagation of 3-D structures with similar parallel and perpendicular scale lengths. In this case, the spacecraft may be entering the structure at the edge of the solitary wave where  $E_{\perp} \sim E_{\parallel}$ , and exiting the structure closer to the center where  $E_{\perp} \ll E_{\parallel}$ .

## 7. Comparison of FAST, Polar, and Viking Results

[41] FAST observations of ion solitary wave velocities contrast sharply with previous estimates. Observations by the Viking satellite of the delay time between current reductions to Langmuir probes separated along the magnetic field suggested that these structures moved much slower than the associated ion beams [Bostrom *et al.*, 1988, 1989]. Koskinen *et al.* [1990] reported that a separate population of cold, slowly moving upgoing ions was present during energetic ion beams. A cold ( $\sim 1-10$  eV) electron population was also indicated by Langmuir probe measurements. The densities of both the cold ions and electrons were estimated to be about 10 times the hot populations. The combined measurements seemed to provide a self-consistent picture of solitary waves as propagating with the cold drifting ions and having small potentials consistent with the cold electron temperature. However, more recent measurements by the FAST spacecraft have shown no evidence of either cold electrons or cold ions [McFadden *et al.*, 1999a], and both Polar and FAST measurements suggest much higher velocity for these structures.

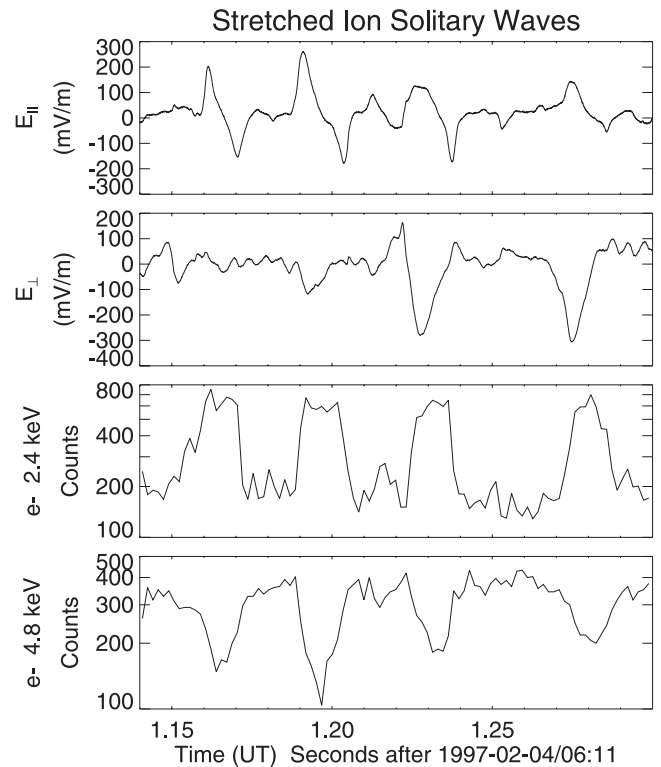


**Figure 13.** The top two panels show the parallel and perpendicular signals during several stretched solitary wave structures, where the electric field goes through an inflection point in the middle of the structure. The bottom panels show the shift in electron counts associated with the waves. These stretched structures appear to have little or no net potential since the electron counts return to prewave levels. Orbit 1804.

[42] Without direct access to the Viking data and a deep understanding of its instruments, it is difficult to determine if these previous reports are in error or if they represent observations in a different plasma regime. The general agreement between plasma observations by FAST and Polar within the auroral acceleration regions strongly suggests the former, so we propose several possible measurement errors that could have resulted in incorrect interpretations of the Viking data. Hilgers *et al.* [1992] showed that the current to the Viking Langmuir probes was dominated by photoelectrons when the probes were aligned along the magnetic field. Thus the 20%–50% current decreases associated with solitary waves by Viking could not have been caused by changes in the local plasma density. They are most likely associated with changes in photoelectron flux induced by the solitary waves as was observed on FAST. The Viking current spike delays were roughly half the solitary wave period, similar to those observed with the FAST current probes, further suggesting the same photoelectron current interaction with the solitary waves. If the Viking observations are the result of solitary wave interactions with photoelectrons, then the resulting velocity estimates are just the antennae length divided by half the wave period, and do not represent a propagation velocity.

[43] McFadden *et al.* [1999a] addressed the Viking reports of cold electrons and cold ions within the density

cavities associated with ion beams. Based upon *Hilgers et al.* [1992] results, McFadden et al. suggested that the cold electron populations were just spacecraft and antennae produced photoelectrons, not ambient plasma. In addition, the cold drifting ion population reported by *Koskinen et al.* [1990] had a flat count rate at low energies. McFadden et al. point out that energetic electrons scattering through ion sensors produce a similar flat background rate. These counts vary in time so they do not appear as a fixed background count rate, and can easily be misinterpreted as an ion flux with substantial density. In light of the more recent FAST and Polar observations, we feel that a reexamination of the Viking results are in order.

[44] The FAST estimates of ion solitary wave velocities also differ from those derived from Polar data. *Dombeck et al.* [2001] found a range of solitary wave velocities that fell within the range of ion beam velocities (100–450 km/s). Relative to the protons, these velocities are about factor of  $\sim 2$  smaller on average than we estimate from FAST. The Polar estimates of parallel phase velocities correspond to rather small (0.1–1.0 ms) time delays in the cross correlation between electric field waveforms that are  $\sim 7$  ms duration and have a sampling resolution of 0.125 ms. As with the Viking data, a detailed comparison of the Polar and FAST observations is beyond the scope of this paper. However, we examined several of the Polar solitary waves and are convinced that the large waveform distortions observed in the FAST short antennae measurements are not present in the Polar data and that the signal delays appear to be adequately resolved.

[45] There are several possible explanations for the difference between Polar and FAST solitary wave velocities. Both observations may be correct and represent altitude variations in the distribution of ion solitary waves. Polar generally makes its measurements at  $>6000$  km, whereas FAST makes its measurements near the bottom of the acceleration region (3000–4000 km). If these structures are short-lived as indicated by some simulations [*Crumley et al.*, 2001], then the generation mechanism is local and could be quite different near the bottom of the acceleration region and deep within the density cavity. In this case the Polar solitary waves may be earthward propagating relative to the proton beam whereas FAST solitary waves are anti-earthward propagating relative to the protons. In section 8 we suggest that the FAST ion solitary waves may result from density fluctuations generated in a double layer at the bottom of the acceleration region. Polar solitary waves appear to be consistent with a two-stream instability between oxygen and hydrogen beams [*Crumley et al.*, 2001].

[46] A second explanation for the Polar-FAST differences is the wave potential versus velocity dependence observed by *Dombeck et al.* [2001]. Since FAST measures much larger amplitude waves, the velocities would be expected to be larger based upon Polar results. However, the Polar trend may have been influenced by errors in the velocity determination since the velocity directly enters the Polar estimates of wave potential. It is not clear how an instability could generate waves whose phase velocity shifts from below to above the proton beam velocity. In addition, FAST observations show no trend between amplitude and velocity, but rather show trends between amplitude and scale size. Therefore we tend to discount any

connection between the larger FAST wave potentials and their higher velocities.

[47] Finally, there is a systematic error that might explain the differences. The solitary waves measured by FAST show distortion most likely caused by changes in photoelectron current to the antennae. This distortion is much smaller for longer antennae, but is still present. The distortion seen in Figure 2 is such that a cross correlation between the V7-V8 and V5-V6 signals would give a nongeophysical long delay time consistent with slower anti-earthward propagation. Much smaller distortions would be expected for the long baseline Polar antennae, but the distortions may still be enough to produce a small nongeophysical delay, resulting in slower phase velocities estimates. If the Polar solitary waves propagate at the beam proton bulk speed plus acoustic speed, their phase velocity would be only slightly higher than the highest velocity portion of the proton beam because of the relatively small  $T_e$ . (We estimate  $\sim 480$  km/s assuming  $T_e \sim 650$  eV, a proton bulk speed equal to 70% of the high-velocity cutoff,  $\sim 400$  km/s, of the proton beam, and 1/3 of the density is in the proton beam.) This velocity is within the error bars of most of the large amplitude events from *Dombeck et al.* [2001]. However, no apparent dependence of the Polar solitary wave velocity versus antennae alignment with the magnetic field is observed (*C. Cattell*, personal communication, 2002) as would be expected if photoelectrons were playing a role in producing nongeophysical signal delays. Thus we discount systematic errors in Polar data as a source of the discrepancy. A more extensive investigation of ion solitary waves on Polar is currently underway and may shed new light on this issue.

[48] In summary, the FAST and Polar observations of auroral ion solitary waves show that these structures propagate near the velocity of the proton beam. The earlier Viking observations of low-velocity solitary waves are highly suspect due to problems with photoelectron currents to their Langmuir probes. Both the FAST and Polar observations are consistent with acoustic modes; however, the FAST waves appear to be propagating anti-earthward relative to the proton beam whereas the Polar waves are propagating earthward relative to the protons. This suggests that different mechanisms are generating acoustic turbulence at the bottom of the acceleration region (FAST) and deep within the acceleration region (Polar).

## 8. Discussion

[49] The FAST observations that ion solitary waves have phase velocities greater than the protons, and consistent with an acoustic mode, should be examined within the context of the particle distribution functions. Figure 14 shows the general shape of the ion and electron distribution functions that are moving up and down the field line. The low-energy cutoff of the  $O^+$  beam and high-energy cutoff of the  $H^+$  beam are at the same energy and reflect the energy gained as these ions passed through a portion of the auroral field-aligned potential drop. Energy exchange between these beams, most likely resulting from the two-stream instability, cause  $O^+$  to form a high-energy tail and  $H^+$  to form a low-energy nearly plateaued distribution function. Hot plasma sheet protons and accelerated auroral electrons that mirror below the spacecraft are also present. The

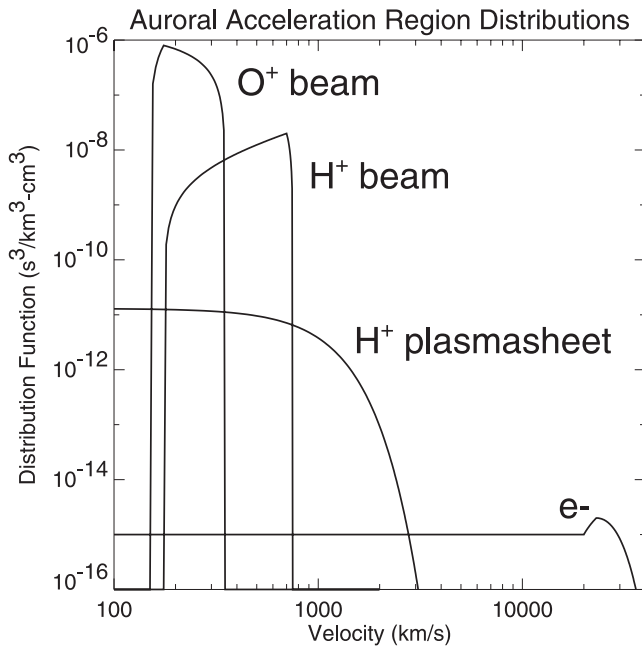


**Figure 14.** The figure illustrates cuts through typical particle distributions observed during ion beams, which often have ion solitary waves. Distribution function values were modeled from orbit 1804. The beams are cuts through the anticarward directed portion which are typically  $10^\circ$  ( $H^+$ ) to  $30^\circ$  ( $O^+$ ) wide, while the plasma sheet  $H^+$  and  $e^-$  are precipitating (earthward directed) and are relatively isotropic except for the loss cone. The  $H^+$  distribution function has a sharp high-energy cutoff at the characteristic beam energy,  $E_c$ ,  $O^+$  has an extended tail above  $E_c$ , the plasma sheet  $H^+$  distribution function is small (even without the loss cone) so that Landau damping is minimal above the  $H^+$  beam peak, and the electrons are nearly plateaued over the ion phase velocities of interest. FAST observations show that the largest amplitude solitary waves are traveling faster than the protons at the  $H^+$  beam peak.

solitary waves measured by FAST appear to propagate at phase velocities just above the proton beam where the primary Landau damping would be from plasma sheet ions and auroral electrons near the loss cone.

[50] To understand ion solitary waves and their role in auroral particle acceleration, a source for these waves needs to be found. Previous theoretical investigations of solitary waves have assumed the structures grew from the free energy available from the two-stream instability caused by  $O^+$  and  $H^+$  falling through a potential drop. However, this instability should give rise to waves whose phase velocity is between the  $O^+$  and  $H^+$  beam velocities. Ion solitary waves observed by Polar are consistent with this two stream instability [Crumley *et al.*, 2001]. Instabilities between the  $H^+$  beam and plasma sheet  $H^+$  would also produce waves propagating earthward relative to the proton beam. Although it may be possible to obtain solitary waves propagating faster than the protons through some nonlinear interaction of the turbulence produced by two-stream instabilities, a simpler solution may result from the nature of the acceleration region as outlined below.

[51] Recent calculations by Ergun *et al.* [2000] have shown that solutions to the Vlasov equation for the upward current acceleration region, using ionospheric and magnetospheric source populations and an imposed potential drop, naturally include localized strong double layers. In particular a strong double layer is often present at the bottom of the acceleration region, forming to reflect secondary electrons in order to keep the ion and electron densities approximately equal within the auroral acceleration cavity. The location and magnitude of this double layer depends upon the ionospheric and magnetospheric source populations. Evidence of the strong double layer is also observed in the particle distributions which show an abrupt increase in ion beam energy as the FAST satellite enters the acceleration region. Typically  $\sim 25\%$  of the field aligned potential drop is observed in the ion beams as FAST traverses the bottom of the acceleration region (M. Temerin *et al.*, The low-altitude extent of the auroral acceleration region in the upward current region as determined by upwardly accelerated ion beams, submitted to *Journal of Geophysical Research*, 2002) This double layer appears to have a corrugated shape, with its altitude varying significantly from flux tube to flux tube [McFadden *et al.*, 1999b]. The corrugation of the double layer is likely due to variations in the ionospheric source populations, which are a complex function of the time history of electron precipitation and wave power on a flux tube.

[52] The ion beam flux and energy can vary by as much as a factor of two on the timescale of the analyzer's energy sweep ( $\sim 78$  ms or  $\sim 400$  m) suggesting that the input flux of conics has similar variations. Even within a single energy sweep, the ion beam spectra can show multiple peaks implying fluctuations much faster than the sweep. These variations are apparent in the top panel of Figure 10 and will produce density fluctuations in the ion beam that will propagate as acoustic waves. Note that large fluctuations in conic flux do not necessarily imply large fluctuations in ion density below the auroral acceleration region where the bulk of the ion density resides in cold plasma.

[53] Acoustic modes of the proton beam will propagate at  $c_s \sim \pm [(n_{H+beam}/n_e)(T_{e||}/m_{H+})]^{1/2}$  relative to the proton bulk speed [Lotko and Kennel, 1983]. For most beam regions the proton beam velocity is greater than  $c_s$  so that both modes move anticarward in the FAST (or earth) reference frame. The prevalence of ion hole solitary waves, or localized rarefactions, implies that either these structures are unusually stable and propagate quite far before dissipating, or that interactions between the conic flux and double layer preferentially generate these localized rarefactions. The observed solitary waves appear to be rarefactions with phase velocities corresponding to the positive sign above. However, some evidence is indicated for acoustic turbulence with the opposite sign. Attempts to integrate the parallel electric field over more than a single solitary structure and compare the result with the potential determined by the electron energy shift were found to have poor agreement. If acoustic turbulence with both phase velocity signs was present, then the integration would fail as observed.

[54] If the solitary waves form out of turbulence at the bottom of the acceleration region, then the structures remaining at higher altitude would be those that survive

propagation of one to several hundred kilometers. Acoustic waves with the negative sign (earthward directed) would have phase velocities that place them within the ion beams where they could grow or be heavily damped. In fact, the formation of large-amplitude earthward directed acoustic waves at the low-altitude double layer may play a role in the rapid momentum exchange between different mass ions. However, once the ions are stabilized (FAST ion distributions indicate significant energy exchange has taken place), growth of earthward directed waves may have been exhausted and these waves may be more heavily damped than the corresponding anti-earthward directed waves because of the larger beam phase space densities. Variations in the ion beam on timescales less than our energy sweep makes wave growth or damping estimates impossible. Simulations of solitary waves arising from the two stream instability [Crumley *et al.*, 2001] give typical lifetimes of only  $\sim 400 \omega_{pe}^{-1} = 40 \omega_{pi}^{-1}$  ( $m_{H^+}/m_e = 100$  for these simulations), with the structures propagating a few to ten times their scale size. For FAST measured densities of  $\sim 0.3 \text{ cm}^{-3}$ ,  $40 \omega_{pi}^{-1} \sim 55 \text{ ms}$ . On the other hand, a calculation of the Landau damping rate for the anti-earthward acoustic waves by the plasma sheet protons, including the loss cone, gives an e-folding damping time of  $\sim 50 \text{ ms}$ . With similar estimates for lifetimes of structures propagating earthward or anti-earthward, the anti-earthward propagating waves would have experienced less damping before arriving at FAST because their phase velocity is directed along the ion beam. This speculation about damping is to remind the reader that since only the largest amplitude waves can be analyzed from the FAST data, the selection process may have determined the anti-earthward velocities observed.

[55] The observation of rarefactions, as opposed to compressions, suggests a stability for these structures. Self-consistent BGK solutions, similar to those for electron solitary waves [Muschiatti *et al.*, 1999], may be possible for rarefactions since rarefactions can form with a trapped population. In this case an ion solitary wave could form out of a decrease in the ion conic flux into the lower border of the acceleration region. The density rarefaction would form as the conics are accelerated into a beam, trapping those plasma sheet ions whose phase velocity is close to the acoustic speed. These nonlinear structures may propagate much farther than would be expected from estimates of the Landau damping rates. Much higher time resolution ion measurements, similar to the SESA instrument used to resolve rapid changes in the electron distribution, may be required to resolve ion distributions within the solitary waves. We note that solitary waves propagating within the proton beam should make a hole in the beam's phase space distribution whereas a solitary wave propagating faster than the proton beam will just reduce the proton's energy in the spacecraft frame during its passage. We plan to perform a detailed study of FAST ion beams to see if any additional information can be extracted from their distributions.

[56] We close by pointing out that ion solitary waves seem to be a byproduct of the auroral acceleration region rather than playing a fundamental role in the acceleration process. Measurements of the electron flux before and after passage of symmetric or asymmetric solitary waves strongly indicate these structures have no significant net potential drop. Therefore these structures are not directly involved in supporting

auroral field aligned potentials, although they may have secondary effects through reflection of auroral electrons and trapping of ions. Many ion beams have no measurable solitary waves further indicating that solitary waves are not essential to the acceleration process. With phase velocities greater than the proton beam, the large amplitude ion solitary waves shown above cannot play a role in momentum exchange between  $H^+$  and heavier ions. Smaller amplitude waves that do play a role in momentum exchange may be present but cannot be resolved from electron energy shifts. The observed waves are consistent with acoustic turbulence propagating anti-earthward relative to the proton beam.

[57] Finally, we are left with several fundamental questions: Can fluctuations in the upgoing conic flux create the solitary waves observed by FAST or is some other mechanism needed? Is there a trapped ion population within the solitary waves? Why do these structures preferentially form relatively symmetric bipolar structures? Are the asymmetric solitary waves due to oblique propagation of 3-D structures, due to time variations, or just due to asymmetric charge distributions? What secondary effects do solitary waves have on the acceleration region through electron reflection? How would fluctuations in ion conic flux affect the lower boundary of the acceleration region? Does motion of the lower boundary of the acceleration region change the ion beam energy through resonant interactions? Could motion of the lower boundary of the acceleration region produce the energy differences between different mass ions? Are the lower-amplitude solitary waves observed by FAST also propagating faster than the proton beam? If not, are they playing a role in momentum exchange between different mass ions? To answer these questions and bring closure to this subject may require much higher-resolution ion measurements than are currently available.

[58] **Acknowledgments.** The analysis of FAST data was supported by NASA grant NAG5-3596.

[59] Arthur Richmond thanks J. P. Crumley and another reviewer for their assistance in evaluating this paper.

## References

- Bergmann, R., and W. Lotko, Transition to unstable ion flow in parallel electric fields, *J. Geophys. Res.*, *91*, 7033, 1986.
- Bostrom, R., G. Gustafsson, B. Holback, G. Holmgren, H. Koskinen, and P. Kintner, Characteristics of solitary waves and weak double layers in the magnetospheric plasma, *Phys. Rev. Lett.*, *61*, 82, 1988.
- Bostrom, R., B. Holback, G. Holmgren, and H. Koskinen, Solitary structures in the magnetospheric plasma observed by Viking, *Phys. Scr.*, *39*, 782, 1989.
- Bounds, S. R., R. F. Pfaff, S. F. Knowlton, F. S. Mozer, M. A. Temerin, and C. A. Kletzing, Solitary potential structures associated with ion and electron beams near  $1 R_E$  altitude, *J. Geophys. Res.*, *104*, 28,709, 1999.
- Carlson, C. W., J. P. McFadden, P. Turin, D. W. Curtis, and A. Magoncelli, The electron and ion plasma experiment for FAST, *Space Sci. Rev.*, *98*, 33, 2001.
- Cattell, C., J. Wygant, J. Dombeck, F. S. Mozer, M. Temerin, and C. T. Russell, Observations of large amplitude parallel electric field wave packets at the plasma sheet boundary, *Geophys. Res. Lett.*, *25*, 857, 1998.
- Crumley, J. P., C. A. Cattell, R. L. Lysak, and J. P. Dombeck, Studies of ion solitary waves using simulations including hydrogen and oxygen beams, *J. Geophys. Res.*, *106*, 6007, 2001.
- Dombeck, J., C. Cattell, J. Crumley, W. K. Peterson, H. L. Collin, and C. Kletzing, Observed trends in auroral zone ion-mode solitary wave structure characteristics using data from Polar, *J. Geophys. Res.*, *106*, 19,013, 2001.
- Ergun, R. E., et al., FAST satellite observations of large-amplitude solitary structures, *Geophys. Res. Lett.*, *25*, 2041, 1998a.
- Ergun, R. E., et al., FAST satellite wave observations in the AKR source region, *Geophys. Res. Lett.*, *25*, 2061, 1998b.

- Ergun, R. E., C. W. Carlson, J. P. McFadden, F. S. Mozer, and R. Strangeway, Parallel electric fields in discrete arcs, *Geophys. Res. Lett.*, *27*, 4053, 2000.
- Ergun, R. E., et al., The FAST satellite fields instrument, *Space Sci. Rev.*, *98*, 67, 2001.
- Hilgers, A., B. Holback, G. Holmgren, and R. Bostrom, Probe measurements of low plasma densities with applications to the auroral acceleration region and auroral kilometric radiation sources, *J. Geophys. Res.*, *97*, 8631, 1992.
- Hudson, M. K., W. Lotko, I. Roth, and E. Witt, Solitary waves and double layers on auroral field lines, *J. Geophys. Res.*, *88*, 916, 1983.
- Klumpar, D. M., et al., The Time-of-Flight Energy Angle, Mass Spectrograph (TEAMS) experiment for FAST, *Space Sci. Rev.*, *98*, 197, 2001.
- Koskinen, H., R. Lundin, and B. Holback, On the plasma environment of solitary waves and weak double layers, *J. Geophys. Res.*, *95*, 5921, 1990.
- Lotko, W., and C. F. Kennel, Spiky ion acoustic waves in collisionless auroral plasma, *J. Geophys. Res.*, *88*, 381, 1983.
- McFadden, J. P., C. W. Carlson, R. E. Ergun, D. M. Klumpar, and E. Moebius, Ion and electron characteristics in auroral density cavities associated with ion beams: No evidence for cold ionospheric plasma, *J. Geophys. Res.*, *104*, 14,671, 1999a.
- McFadden, J. P., C. W. Carlson, and R. E. Ergun, Microstructure of the auroral acceleration region as observed by FAST, *J. Geophys. Res.*, *104*, 14,453, 1999b.
- Moebius, E., et al., Species-dependent energies in upward directed ion beams over auroral arcs as observed with FAST TEAMS, *Geophys. Res. Lett.*, *25*, 2029, 1998.
- Muschietti, L., I. Roth, R. E. Ergun, and C. W. Carlson, Analysis and simulation of BGK electron holes, *Nonlinear Process. Geophys.*, *6*, 211, 1999.
- Muschietti, L., I. Roth, C. W. Carlson, and M. Berthomier, Modeling stretched solitary waves along magnetic field lines, *Nonlinear Process. Geophys.*, *9*, 101, 2002.
- Roennmark, K., Computation of the dielectric tensor of a Maxwellian plasma, *Plasma Phys.*, *25*, 699, 1983.
- Strangeway, R. J., et al., FAST observations of VLF waves in the auroral zone: Evidence of very low plasma densities, *Geophys. Res. Lett.*, *25*, 2065, 1998.
- Temerin, M., K. Cerney, W. Lotko, and F. S. Mozer, Observations of double layers and solitary waves in auroral plasma, *Phys. Rev. Lett.*, *48*, 1175, 1982.
- Tran, M. Q., Ion acoustic solitons in a plasma: A review of their experimental properties and related theories, *Phys. Scr.*, *20*, 317, 1979.
- 
- C. W. Carlson, J. P. McFadden, F. S. Mozer, L. Muschietti, and I. Roth, Space Sciences Laboratory, University of California, Berkeley, CA 94720-7450, USA. (cwc@ssl.berkeley.edu; mcfadden@ssl.berkeley.edu; fmozer@ssl.berkeley.edu; laurent@ssl.berkeley.edu; ilan@ssl.berkeley.edu)
- R. E. Ergun, LASP, University of Colorado, Boulder, CO 80303, USA. (ree@fast.colorado.edu)
- E. Moebius, Institute for the Study of Earth, Oceans, and Space, University of New Hampshire, Durham, NH 93824, USA. (Eberhard.Moebius@unh.edu)